MORE ACCURATE HYBRID PO-MOM ANALYSIS FOR AN ELECTRICALLY LARGE ANTENNA-RADOME STRUCTURE

B. Hu, X. Xu, M. He, and Y. Zheng

Department of Electronic Engineering
Beijing Instititive of Technology
Beijing 100081, China

Abstract—More accurate hybrid PO-MOM process combining physical optics (PO) with method of moment (MOM) is employed to analyze an electrically large antenna-radome structure. The mutual interactions among the antenna, the inner and outer surfaces of the radome are considered through a group of associated integral equations. In the analysis, the antenna surface and the sharp tip part on the radome surface are modeled accurately by using MOM while the rest smooth parts on the radome surfaces are approximated by using PO. Numerical results indicate that the hybrid process presented in this paper is much more accurate than the conventional PO-MOM ones.

1. INTRODUCTION

The dielectric radome is usually used to protect the antenna and the electrical system from various damages and disturbances [1]. However, the radome also affects the antenna radiation pattern, for the existence of equivalent electric and magnetic currents on the surface of radome wall [2]. For an antenna-radome structure, the precise numerical model can be established by using method of moments (MOM) [3–5]. Unfortunately, the MOM analysis costs so large amount of computer memory and CPU time that the conventional personal computer can not accomplish the task, when the electrical size of the radome is very large, though some accelerating methods could be adopted [6–8]. Some high frequency techniques are suitable for electrically large radomes [9, 10] but not accurate for discontinuous structures on the

---

Corresponding author: B. Hu (hubing@bit.edu.cn).

radome surfaces. Recently, a hybrid method combining physical optics (PO) and MOM together, PO-MOM, has been introduced to deal with the intractable problem and proved to be efficient [11, 12]. However, the mutual interaction between the antenna and radome was either ignored [11] or partly ignored [12]. As a result, the numerical results are not very convincing. In this paper, the more accurate an improved PO-MOM hybrid process is developed to investigate an electrically large radome-antenna structure. In the analysis, the antenna and radome are considered as a whole, so that the integral equations include the mutual coupling information among the antenna, the inner and outer surfaces of the radome. The antenna surface and the tip parts of radome surfaces are modeled as MOM regions, and the rest smooth parts of the radome surfaces are done as PO regions. In addition, only the first order mutual coupling effects are considered when evaluating the PO currents by counting the cost of the accuracy and efficiency of the analysis. Numerical results indicate that the more accurate hybrid PO-MOM process is much more appropriate than the former PO-MOM methods for the analysis of electrically large antenna-radome structures, especially for moderate size or complex ones.

2. THEORY AND FORMULATION

2.1. Integral Equation and MOM

Figure 1 shows the geometry of an antenna enclosed in an arbitrary shape radome. Considering the coupling among the antenna, and the inner and outer surface of the radome, the electric and magnetic field integral equations can be derived by using Maxwell's equations and the boundary conditions on different surfaces, that is,

$$\left[\vec{E}_1^1\left(\vec{J}_1\right)+\vec{E}_2^1\left(\vec{J}_2,\vec{M}_2\right)\right]_{1\,\tan}=-\vec{E}_{1\,\tan}^i \tag{1}$$

$$\left[\vec{E}_1^1\left(\vec{J}_1\right)+\vec{E}_2^1\left(\vec{J}_2,\vec{M}_2\right)+\vec{E}_2^2\left(\vec{J}_2,\vec{M}_2\right)+\vec{E}_3^2\left(\vec{J}_3,\vec{M}_3\right)\right]_{2\,\tan}=0 \tag{2}$$

$$\left[\vec{H}_1^1\left(\vec{J}_1\right)+\vec{H}_2^1\left(\vec{J}_2,\vec{M}_2\right)+\vec{H}_2^2\left(\vec{J}_2,\vec{M}_2\right)+\vec{H}_3^2\left(\vec{J}_3,\vec{M}_3\right)\right]_{2\,\tan}=0 \tag{3}$$

$$\left[\vec{E}_2^2\left(\vec{J}_2,\vec{M}_2\right)+\vec{E}_3^2\left(\vec{J}_3,\vec{M}_3\right)+\vec{E}_3^3\left(\vec{J}_3,\vec{M}_3\right)\right]_{3\,\tan}=0 \tag{4}$$

$$\left[\vec{H}_2^2\left(\vec{J}_2,\vec{M}_2\right)+\vec{H}_3^2\left(\vec{J}_3,\vec{M}_3\right)+\vec{H}_3^3\left(\vec{J}_3,\vec{M}_3\right)\right]_{3\,\tan}=0 \tag{5}$$

where $\vec{E}_\alpha^\beta(\vec{J}_\alpha, \vec{M}_\alpha)$ and $\vec{H}_\alpha^\beta(\vec{J}_\alpha, \vec{M}_\alpha)$ represent the electric field and the magnetic field, respectively, in the βth region ($\beta = 1, 2, 3$) generated by the corresponding electric current $\vec{J}_\alpha$ and magnetic current $\vec{M}_\alpha$ on the αth surface ($\alpha = 1, 2, 3$). Employing the Galerkin's procedure of MOM, the above-mentioned integral equations are converted to the following matrix equation, i.e.,

$$
\begin{bmatrix}
[Z_{11}] \cdot [Z_{12}] \cdot [C_{12}] \cdot [Z_{13}] \cdot [C_{13}] \\
[Z_{21}] \cdot [Z_{22}] \cdot [C_{22}] \cdot [Z_{23}] \cdot [C_{23}] \\
[D_{21}] \cdot [D_{22}] \cdot [Y_{22}] \cdot [D_{23}] \cdot [Y_{23}] \\
[Z_{31}] \cdot [Z_{32}] \cdot [C_{32}] \cdot [Z_{33}] \cdot [C_{33}] \\
[D_{31}] \cdot [D_{32}] \cdot [Y_{32}] \cdot [D_{33}] \cdot [Y_{33}]
\end{bmatrix}
\cdot
\begin{bmatrix}
[I_1] \\
[I_2] \\
[M_2] \\
[I_3] \\
[M_3]
\end{bmatrix}
=
\begin{bmatrix}
[V_1] \\
[0] \\
[0] \\
[0] \\
[0]
\end{bmatrix}
\quad (6)
$$

where Z, Y, C, D, I, M, V have the same meanings as those in [13], the subscripts 1, 2 and 3 represent the serial number of the three surfaces in the MOM model shown in Fig. 1.
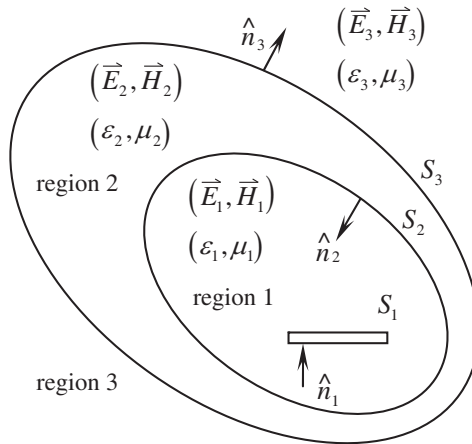

Figure 1. The geometry of an antenna enclosed in an arbitrary shape radome.

Although the above MOM model is exact in theory for the antenna-radome structure, it becomes very inefficient in the numerical computation when the structure size is increasingly large compared to the operating wavelength. To overcome this difficulty while keeping enough numerical accuracy, the hybrid PO-MOM method combining PO and MOM together is introduced and improved by considering more accurately the mutual couplings between the PO regions and the MOM ones on the boundary surfaces of the structure, not only

including the effects between the antenna surface and the radome surfaces but also including those between the MOM regions on the radome surfaces and the PO regions on them.

2.2. More Accurate Hybrid PO-MOM Process

Considering the accuracy and efficiency, the whole antenna surface and the regions varying sharply on the inner and outer surfaces of the radome are modeled as MOM regions while the regions varying smoothly are done as PO regions. As same as in [14], the triangles of the MOM regions are also grouped by the common edge of two adjacent triangles, and therefore a pair of adjacent triangles is included in each group. On the other hand, the triangles of PO regions are grouped as usual by a single triangle, that is, each group contains only one triangle.

Assume $\vec{J}_\alpha^{MoM}$ and $\vec{M}_\alpha^{MoM}$ to be the MOM electric and magnetic current on the three different surfaces of the MOM regions, and $\vec{J}_\alpha^{PO}$ and $\vec{M}_\alpha^{PO}$ to be the corresponding PO currents on those of the PO regions. $\vec{J}_\alpha^{MoM}$ and $\vec{M}_\alpha^{MoM}$ can be expressed by RWG basic functions [14], i.e., $\vec{J}_\alpha^{MoM} = \sum_{n=1}^{N_\alpha^{MoM}} I_{\alpha,n} \vec{f}_{\alpha,n}$ and $\vec{M}_\alpha^{MoM} = \sum_{n=1}^{N_\alpha^{MoM}} M_{\alpha,n} \vec{f}_{\alpha,n}$, where $\vec{f}_{\alpha,n}$ is defined on the αth surface, N_α^{MoM} is the number of the common edges of the MOM region(s) on the αth surface. On the other hand, $\vec{J}_\alpha^{PO}$ and $\vec{M}_\alpha^{PO}$ can be expressed simply by pulse functions. Strictly, the ingredients of $\vec{J}_\alpha^{PO}$ and $\vec{M}_\alpha^{PO}$ must include the contributions from all MOM currents. However, the analysis shows that the contribution of the electromagnetic field produced by the antenna electric current $\vec{J}_1^{MoM}$ is the first order and main effect, while those produced by the MOM currents $\vec{J}_2^{MoM}$, $\vec{M}_2^{MoM}$, $\vec{J}_3^{MoM}$ and $\vec{M}_3^{MoM}$ on the inner and outer surfaces of the radome are only the second or even higher order smaller ones. Consequently, balancing the computation cost and the accuracy, only the first order effect is considered here in the analysis, and the numerical results in Section 3 will indicate that the approximation is appropriate.

Based on above analysis, the first column of sub-matrices in the impedance matrix of Eq. (6) should be modified and written in the

following forms:

$$[Z_{11}] = \left[Z_{11}^{MoM}\right] + \left[Z_{11}^{PO}\right]$$
$$[Z_{21}] = \left[Z_{21}^{MoM}\right] + \left[Z_{21}^{PO}\right] \quad [D_{21}] = \left[D_{21}^{MoM}\right] + \left[D_{21}^{PO}\right]$$
$$[Z_{31}] = \left[Z_{31}^{MoM}\right] + \left[Z_{31}^{PO}\right] \quad [D_{31}] = \left[D_{31}^{MoM}\right] + \left[D_{31}^{PO}\right]$$

where $\left[Z_{11}^{MoM}\right]$, $\left[Z_{21}^{MoM}\right]$, $\left[D_{21}^{MoM}\right]$, $\left[Z_{31}^{MoM}\right]$ and $\left[D_{31}^{MoM}\right]$ are calculated by normal MOM process, while $\left[Z_{11}^{PO}\right]$, $\left[Z_{21}^{PO}\right]$, $\left[D_{21}^{PO}\right]$, $\left[Z_{31}^{PO}\right]$ and $\left[D_{31}^{PO}\right]$ are evaluated by the improved PO-MOM process based on Eqs. (1)–(5). And the final results can be expressed by the following formulas:

$$Z_{11,mn}^{PO} = \Omega_{2,1}^1$$
$$Z_{21,mn}^{PO} = \Omega_{2,2}^1 + \Omega_{2,2}^2 + \Omega_{3,2}^2 \quad D_{21,mn}^{PO} = \Theta_{2,2}^1 + \Theta_{2,2}^2 + \Theta_{3,2}^2$$
$$Z_{31,mn}^{PO} = \Omega_{2,3}^2 + \Omega_{3,3}^2 + \Omega_{3,3}^3 \quad D_{31,mn}^{PO} = \Theta_{2,3}^2 + \Theta_{3,3}^2 + \Theta_{3,3}^3$$

where

$$\Omega_{\alpha,\varsigma}^{\beta} = \frac{-j\omega\mu_\beta l_{\varsigma,m}}{8\pi} \sum_{k=1}^{N_\alpha^{PO}} S_{\alpha,k}^{PO} \vec{\gamma}_{\alpha,k,n}^{PO} \cdot \left[\vec{\rho}_{\varsigma,m}^{c+} \cdot G_\beta \left(\vec{r}_{\varsigma,m}^{c+}, \vec{r}_{\alpha,k}^{c} \right) \right.$$

$$\left. + \vec{\rho}_{\varsigma,m}^{c-} \cdot G_\beta \left(\vec{r}_{\varsigma,m}^{c-}, \vec{r}_{\alpha,k}^{c} \right) \right] + \frac{l_{\varsigma,m}}{8\pi} \sum_{k=1}^{N_\alpha^{PO}} S_{\alpha,k}^{PO} \vec{\tau}_{\alpha,k,n}^{PO}$$

$$\cdot \left[\vec{\rho}_{\varsigma,m}^{c+} \times \nabla' G_\beta \left(\vec{r}_{\varsigma,m}^{c+}, \vec{r}_{\alpha,k}^{c} \right) + \vec{\rho}_{\varsigma,m}^{c-} \times \nabla' G_\beta \left(\vec{r}_{\varsigma,m}^{c-}, \vec{r}_{\alpha,k}^{c} \right) \right] \quad (7)$$

$$\Theta_{\alpha,\varsigma}^{\beta} = \frac{-j\omega\varepsilon_\beta l_{\varsigma,m}}{8\pi} \sum_{k=1}^{N_\alpha^{PO}} S_{\alpha,k}^{PO} \vec{\tau}_{\alpha,k,n}^{PO} \cdot \left[\vec{\rho}_{\varsigma,m}^{c+} \cdot G_\beta \left(\vec{r}_{\varsigma,m}^{c+}, \vec{r}_{\alpha,k}^{c} \right) \right.$$

$$\left. + \vec{\rho}_{\varsigma,m}^{c-} \cdot G_\beta \left(\vec{r}_{\varsigma,m}^{c-}, \vec{r}_{\alpha,k}^{c} \right) \right] - \frac{l_{\varsigma,m}}{8\pi} \sum_{k=1}^{N_\alpha^{PO}} S_{\alpha,k}^{PO} \vec{\gamma}_{\alpha,k,n}^{PO}$$

$$\cdot \left[\vec{\rho}_{\varsigma,m}^{c+} \times \nabla' G_\beta \left(\vec{r}_{\varsigma,m}^{c+}, \vec{r}_{\alpha,k}^{c} \right) + \vec{\rho}_{\varsigma,m}^{c-} \times \nabla' G_\beta \left(\vec{r}_{\varsigma,m}^{c-}, \vec{r}_{\alpha,k}^{c} \right) \right] \quad (8)$$

In Eq. (7) and Eq. (8), $G_\beta(\vec{r}, \vec{r}') = e^{-jk_\beta R}/R$ is the Green's function in βth region, k_β is the wave-number in the corresponding medium region, $l_{\varsigma,m}$ is the length of the mth common edge on the ςth surface, $\vec{r}_{\varsigma,m}^{c+}$ and $\vec{r}_{\varsigma,m}^{c-}$ are the centroids of the mth pair of adjacent triangles, $\vec{\rho}_{\varsigma,m}^{c+}$ and $\vec{\rho}_{\varsigma,m}^{c-}$ are the vectors between the free vertexes and

the centroids of the mth pair of adjacent triangles. In addition, N_α^{PO} is the number of the triangles of the PO region on the αth surface, $S_{\alpha,k}^{PO}$ is the area of the kth triangle on the αth surface, $\vec{r}_{\alpha,k}^{\,c}$ is the centroid of the kth triangle, $\vec{\gamma}_{\alpha,k,n}^{PO}$ and $\vec{\tau}_{\alpha,k,n}^{PO}$ are the equivalent currents on kth triangle on the radome produced by the fields originated from the source $\vec{f}_{\varsigma,n}$ on the ςth surface.

Recently, two hybrid PO-MOM approaches for the analysis of the antenna-radome structure have been reported [11, 12]. In [11], the sharp tip of the radome is calculated by MOM, while the smooth part by PO method. Unfortunately, the mutual interaction between the antenna and the radome is ignored in the analysis, so this kind of approximation is too rough for a medium size radiation structure. In [12], the disadvantage in [11] is made up, but another problem is introduced, that is, the mutual interaction of the sharp tip parts on the radome surfaces is neglected, which is not appropriate for a complex radome.

For the above imore accurate hybrid PO-MOM process, the mutual interactions among the antenna surface, the inner and outer surface of the radome are all considered in the associated integral equations (Eqs. (1)–(5)). During the computing process, the sharp parts of the radome and the antenna are modeled as MOM region to ensure higher accuracy while the rest smooth parts are dealt with PO method to increase computational efficiency. Therefore, hybrid PO-MOM process presented in this paper should be more applicable.

3. NUMERICAL RESULTS

As shown in Fig. 2, the radome-antenna structure is composed of a dipole antenna array and an electrically large dielectric radome. The radome is a half rotation-ellipsoid shell, with a and b each representing the half-length of the minor and major semi-axis of its outer surface. In addition, the major semi-axis of the radome is fixed along the x-axis, and t and ε_r will be used to show the thickness and the relative permittivity of the dielectric radome, respectively. The antenna array considered in the analysis comprises five center-fed cylindrical dipole elements, each has the length of 0.47λ and the diameter of 0.0025λ, being aligned along z direction with the spacing of 0.6λ in between, wherein λ stands for the working wavelength of the antenna. The equivalent strip model [15] is employed in the analysis. As shown in Fig. 2, m defines the tip depth of the MOM regions on the radome surfaces, and h is the distance between the radome bottom and the linear dipole array.
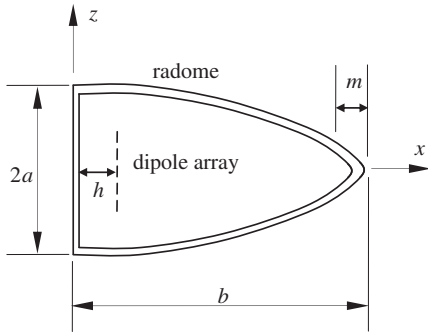
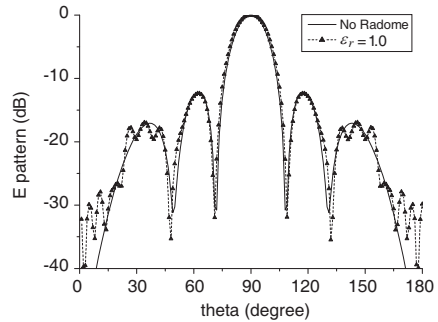**Figure 2.** Geometry of a linear array enclosed in a half rotation-ellipsoid radome.

Figure 3. Comparison of E plane pattern between the antenna array without radome and with a transparent radome ($\varepsilon_r = 1.0$).

Firstly, the validation of the hybrid PO-MOM process in this paper is presented. Fig. 3 shows the E-plane radiation patterns for the linear dipole array with a transparent half rotation-ellipsoid radome ($\varepsilon_r = 1.0$), wherein $a = 5$, $b = 10$, $h = 2\lambda$, $m = 0.25\lambda$, $t = 0.1\lambda$. The tip part of the radome and the antenna are all selected to be MOM regions. When the RWG basic function is applied in the MOM region, the side lengths of the triangle facets on the radome are about 0.1λ, and those of the antenna are about 0.015λ. For the PO region, the lengths of the side are about 0.25λ. As seen in Fig. 3, there is good agreement between the cases of no radome and with a transparent radome. So the improved hybrid PO-MOM method is accurate enough for such radiation system.

Figure 4 shows the E-plane radiation patterns for different permittivities of the dielectric radome when $h = 2\lambda$, $m = 0.25\lambda$ and $t = 0.1\lambda$. Fig. 5 shows the E-plane radiation patterns for different thicknesses of the radome when $h = 2\lambda$, $m = 0.25\lambda$, and $\varepsilon_r = 2.5$. The segmentation rules are the same as those in Fig. 3. It can be seen from the two figures that the side lobe are affected significantly by the permittivity and the thickness of the semi-rotation-ellipsoid radome.

Compared with the hybrid methods presented in [11] and [12], the improved hybrid method can present finer result because more mutual information considered. Fig. 6 shows the comparison of the hybrid method in this paper with those presented in [11] and [12]. The antenna and radome structure is shown in Fig. 2, and the detailed geometrical parameters are the same as those in the example of Fig. 4, except for $\varepsilon_r = 4.2$.
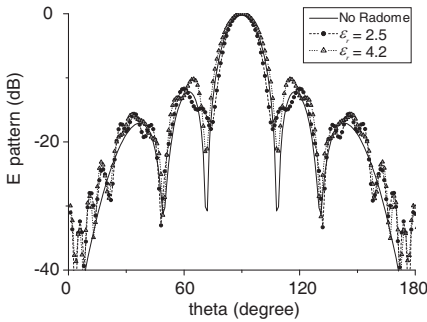
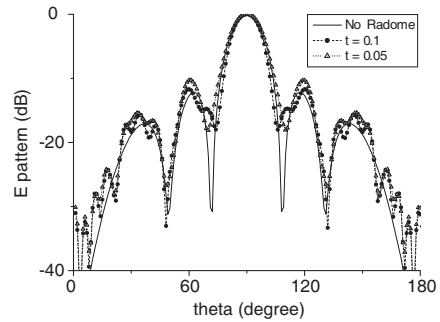**Figure 4.** *E* plane pattern vs. the permittivity of radome.

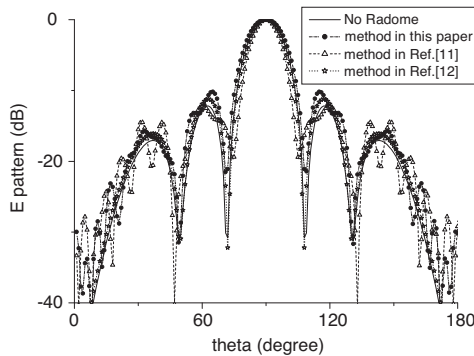**Figure 5.** *E* plane pattern vs. the thickness of radome.

Figure 6. Comparison for *E* plane patterns derived by different hybrid methods.

It can be seen from Fig. 6 that the first side lobe changes significantly for the result of the improved method, while the results of the other two hybrid methods show little variation.

Furthermore, in the near field analysis for the same structure, hybrid method in this paper shows more obviously different results than those presented in [11] and [12]. Table 1 presents the input impedances of the antenna array with and without the dielectric radome. The five antenna array elements are numbered 1 to 5 along z-axis. Only the input impedances of the first three elements are considered due to symmetry.

Obvious differences between the input impedances of the array with and without the dielectric radome ($\varepsilon_r = 2.5$, 4.2) are noted in Table 1. The results of method in [11] show no change compared with the case of no radome because the mutual interaction between

Table 1. Comparison for input impedances of different hybrid methods ($t = 0.1\lambda$).

The number of elements		1	2	3
No Radome		$81.24 - j\,8.93$	$95.29 - j\,25.49$	$94.85 - j\,10.17$
With Radome ($\varepsilon_r = 2.5$)	Ref. [11]	$81.24 - j\,8.93$	$95.29 - j\,25.49$	$94.85 - j\,10.17$
	Ref. [12]	$80.56 - j\,16.89$	$100.88 - j\,29.42$	$98.19 - j\,9.41$
	This paper	$82.66 - j\,16.98$	$103.98 - j\,27.65$	$99.89 - j\,7.03$
With Radome ($\varepsilon_r = 4.2$)	Ref. [11]	$81.24 - j\,8.93$	$95.29 - j\,25.49$	$94.85 - j\,10.17$
	Ref. [12]	$76.72 - j\,22.71$	$101.49 - j\,38.56$	$102.71 - j\,16.18$
	This paper	$80.33 - j\,23.20$	$107.54 - j\,36.11$	$106.59 - j\,12.05$

Table 2. Comparison for efficiency of different methods.

Method	Number of unknown (MOM)	Number of unknown (PO)	CPU time
Ref. [11]	2000	0	5 minute 21 s
Ref. [12]	235	41932	21 minute 26 s
This paper	2235	82472	4 hr. 22 minute 13 s

the antenna and radome is neglected; and the results of method in this paper present more obvious change than those in [12] because the associated integral equations (Eqs. (1)–(5)) include more coupling information.

The comparisons in Fig. 6 and Table 1 indicate that hybrid PO-MOM method in this paper are more accurate. Therefore, the more coupling information also consume more computer resources. Table 2 shows the comparison of different methods in computer costs. Compared with the hybrid methods presented in [11] and [12], hybrid method in this paper takes much more CPU time and computer memories, but such costs are worthwhile for the not very large or complex antenna-radome structure because more coupling information should be considered.

4. CONCLUSION

In this paper, the more accurate hybrid PO-MOM process is presented, which is suitable for the analysis of electrically large antenna-radome structures, especially for moderate size or complex ones. In this method, the antenna surface and the sharp tip parts on the radome surfaces are modeled more accurately as the MOM regions, while the

smooth parts left on the radome surfaces are approximated as the PO regions. The mutual interactions among the antenna surface, the inner and outer surface of the radome are all considered through a group of associated integral equations. Numerical results indicate that the hybrid PO-MOM method in this paper is much more accurate than the former PO-MOM ones for antenna-radome structures.

REFERENCES

1. Oğuzer, T. and A. Altintas, "Analysis of the nonconcentric reflector antenna-in-radome system by the iterative reflector antenna and radome interaction," *Journal of Electromagnetic Waves and Applications*, Vol. 21, No. 1, 57–70, 2007.

2. Sukharevsky, O. I. and V. A. Vasilets, "Scattering of reflector antenna with conic dielectric radome," *Progress In Electromagnetics Research B*, Vol. 4, 159–169, 2008.

3. Arvas, E., A. Rahhalarabi, U. Pekel, and E. Gundogan, "Electromagnetic transmission through a small radome of arbitrary shape," *IEE Proceedings H*, Vol. 137, 401–405, 1990.

4. Zou, Y. L., J. Y. Li, and Q. Z. Liu, "Modified mode decomposition for analyzing antennas with body of revolution radome," *Journal of Electromagnetic Waves and Applications*, Vol. 21, No. 10, 1403–1410, 2007.

5. Zou, Y., Q. Liu, and J. Guo, "Fast analysis of body-of-revolution radomes with method of moments," *Journal of Electromagnetic Waves and Applications*, Vol. 21, No. 13, 1803–1817, 2007.

6. Nie, X.-C. and N. Yuan, L.-W. Li and T.-S. Yeo, and Y.-B. Gan, "Fast analysis of electromagnetic transmission through arbitrarily shaped airborne radomes using precorrected-FFT method," *Progress In Electromagnetics Research*, PIER 54, 37–59, 2005.

7. Yuan, N., X.-C. Nie, Y.-B. Gan, T.-S. Yeo, and L.-W. Li, "Accurate analysis of conformal antenna arrays with finite and curved frequency selective surfaces," *Journal of Electromagnetic Waves and Applications*, Vol. 21, No. 13, 1745–1760, 2007.

8. Lu, C.-C., "A fast algorithm based on volume integral equation for analysis of arbitrarily shaped dielectric radomes," *IEEE*

Transaction on Antennas and Propagation, Vol. 51, 606–612, Mar. 2003.

9. Shifflett, J. A., "CADDRAD: A physical optics radar/radome analysis code for arbitrary 3D geometries," *IEEE Antennas Propagation Magazine*, Vol. 39, 73–79, Dec. 1997.

10. Hémon, R., P. Pouliguen, H. He, J. Saillard, and J.-F. Damiens, "Computation of EM field scattered by an open-ended cavity and by a cavity under radome using the iterative physical optics," *Progress In Electromagnetics Research*, PIER 80, 77–105, 2008.

11. Abdel Moneum, M. A., Z. Shen, J. L. Volakis, and O. Graham, "Hybrid PO-MOM analysis of large axi-symmetric radomes," *IEEE Transaction on Antennas and Propagation*, Vol. 49, 1657–1666, 2001.

12. Zhao, W.-J., Y.-B. Gan, L.-W. Li, and C.-F. Wang, "Effects of an electrically large airborne radome on radiation patterns and input impedance of a dipole array," *IEEE Transaction on Antennas and Propagation*, Vol. 55, 2309–2402, Aug. 2007.

13. Umashankar, K., A. Taflove, and S. M. Rao, "Electromagnetic scattering by arbitrary shaped three-dimensional homogeneous lossy dielectric objects," *IEEE Transaction on Antennas and Propagation*, Vol. 34, 758–766, 1986.

14. Rao, S. M., D. R. Wilton, and A. W. Glison, "Electromagnetic scattering by surfaces of arbitrary sharp," *IEEE Transaction on Antennas and Propagation*, Vol. 30, 409–418, 1982.

15. Makarov, S. N., *Antenna and EM Modeling with MATLAB*, 4–10, Wiley, New York, 2002.